Energy 173 (2019) 1256–1272

Contents lists available at ScienceDirect

Energy

journal homepage: www.elsevier.com/locate/energy

Dual fluidized bed steam gasification: Change of product gas quality along the reactor height

A.M. Mauerhofer*, J.C. Schmid, F. Benedikt, J. Fuchs, S. Müller, H. Hofbauer

Institute of Chemical, Environmental and Bioscience Engineering, TU Wien, 1060, Vienna, Austria

ARTICLE INFO

Article history:
Received 8 October 2018
Received in revised form
8 January 2019
Accepted 3 February 2019
Available online 11 February 2019

Keywords:
Dual fluidized bed
Gasification
Counter-current column
Combustion
Gas-solid interaction
Tar destruction

ABSTRACT

The impact of the counter-current column of the gasification reactor of a 100 kW_{th} dual fluidized bed steam gasification pilot plant on the product gas quality was investigated. Through the advanced design of the gasification reactor by operating the lower part as bubbling bed and the upper part as counter-current column, the gas-solid interactions between downward flowing hot bed material particles with upwards flowing product gas could be enhanced. This was realized by equipping the counter-current column with constrictions, which increase the residence time and the bed material hold-up. Thus, the conversion efficiency of the fuel including the tar was improved. For the investigations three different experimental campaigns converting softwood pellets using a mixture of olivine and limestone (50/50 wt.-%), a mixture of feldspar and limestone (50/50 wt.-%), and 100 wt.-% quartz as bed materials were conducted. Higher H_2 contents and lower contents of higher hydrocarbons could be detected along the height of the counter-current column. Especially heavy tar compounds could be reduced significantly. These two effects are explained by enhanced water gas shift and steam reforming reactions. In case of catalytically inactive quartz, only thermal effects are available and therefore lower effects on tar reduction could be obtained.

1. Introduction

The forecast of an increase of the global energy demand up to 70% as well as a raise of carbon dioxide (CO_2) emissions up to 60% in 2050 compared to 2011, drives the research on renewable energy systems and technologies to a huge extent [1]. Due to the fact, that today's energy demand is mainly covered by fossil fuels worldwide high greenhouse gas emissions are released [2]. To reduce the release of greenhouse emissions and to mitigate the negative effects on the climate change, the amount of renewables in our energy system has to be increased. Therefore, research and implementation of sustainable production processes of biogenic feedstocks are becoming more and more relevant. One way of a sustainable, environmental-friendly production presents the thermo-chemical conversion. The thermo-chemical conversion process "gasification" converts solid feedstocks into a valuable product gas. Especially, the dual fluidized bed (DFB) steam gasification has a great potential in this respect and is, therefore, a main research topic at TU Wien since many years. In Figs. 1 and 2, the basic principles of the dual fluidized bed steam gasification are shown.

The DFB "classic" steam gasification (Fig. 1) is composed of two reactors, a gasification reactor (GR; blue rectangle) and a combustion reactor (CR; red rectangle). These two reactors are connected through loop seals. A bed material circulates between the GR and CR. This bed material serves as a heat carrier from the combustion reactor to the gasification reactor to enable the endothermic steam gasification. In the "classic" design, devolatilization and gasification reactions between 750 and 850 °C take place.

The "advanced" gasification reactor (Fig. 2) is divided into two parts: i) a lower part with the devolatilization and gasification process at temperatures of around 750–850 °C and ii) an upper part, where reforming and tar cracking reactions at temperatures of around 900–970 °C take place. In the gasification reactor, a high valuable product gas is generated. Conversely, in the combustion reactor a flue gas is produced in an oxidizing atmosphere at temperatures of around 900–1000 °C. The use of steam as fluidization agent in the gasification reactor enables to generate a nitrogen-free product gas, which is mainly composed of hydrogen (H_2), carbon monoxide (CO), CO_2, methane (CH_4), ethylene (C_2H_4), and other

* Corresponding author.
E-mail addresses: anna.mauerhofer@tuwien.ac.at (A.M. Mauerhofer), johannes.schmid@tuwien.ac.at (J.C. Schmid), florian.benedikt@tuwien.ac.at (F. Benedikt), josef.fuchs@tuwien.ac.at (J. Fuchs), stefan.mueller@tuwien.ac.atand (S. Müller), hermann.hofbauer@tuwien.ac.at (H. Hofbauer).

https://doi.org/10.1016/j.energy.2019.02.025

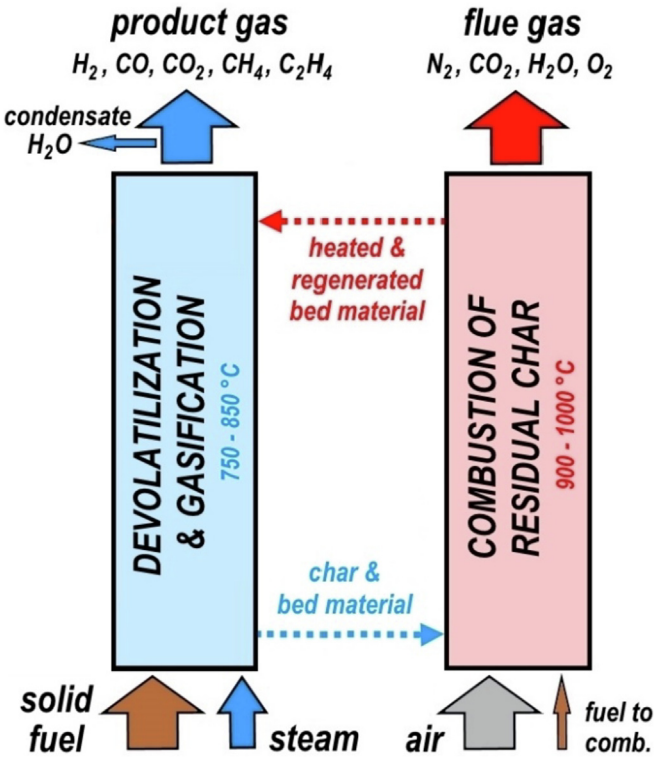

Fig. 1. Fundamental principle of the classic dual fluidized bed steam gasification.

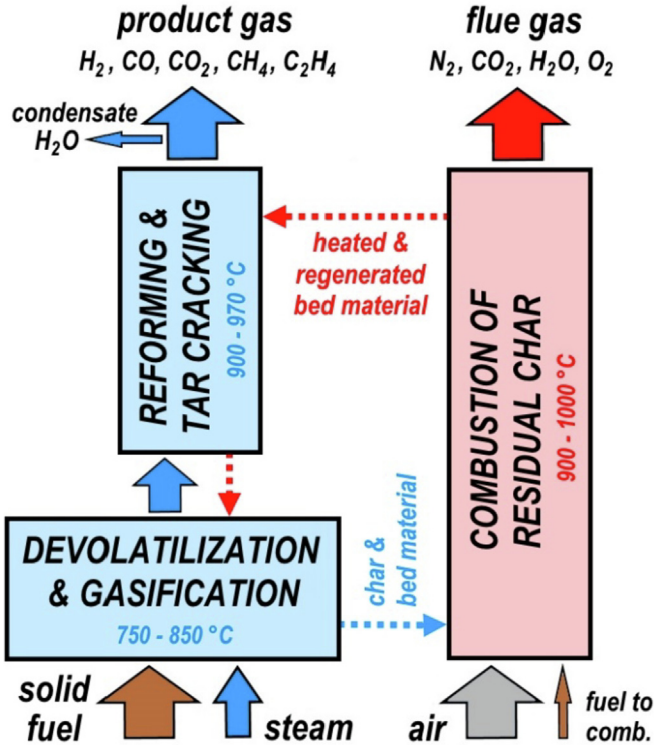

Fig. 2. Fundamental principle of the advanced dual fluidized bed steam gasification.

minor components. On the one hand, the product gas can be used for generation of heat and electricity [3]. On the other hand, the product gas can also be applied in different synthesis to produce fuels such as FT-fuels or chemicals like mixed alcohols [4].

In the 1990's, the dual fluidized bed steam gasification was developed successfully with the construction of a 100 kW_{th} pilot plant at TU Wien [5]. Between 2002 and 2014 industrial-sized plants followed with an increasing fuel power from 8 MW_{th} to 32 MW_{th} in Austria, Germany and Sweden. More detailed descriptions can be found in Refs. [6–8].

The focus of this paper is to investigate the effects of the counter-current column of the upper part of the gasification reactor on i) the product gas composition and ii) tar formation/destruction. Product gas and tar measurements before (lower sample point, LSP) and after (upper sample point, USP) the counter-current column have already been conducted in the last years (see Fig. 3). Results of these measurements showed, that the counter-current column has a remarkable effect on the product gas composition (see literature [9,10]). However, the product gas measurement including tar formation along the counter-current column has not been carried out till now. So, to gain detailed information about the processes taking place along the height of the column, specific measurements were carried out within this work. For this purpose, measurements at in total eleven measurement points along the height of the gasification reactor were carried out. In Fig. 3 the gasification reactor with the measurement points (red dashed lines) is displayed. For test campaign 1, the product gas composition was measured at all eleven measurement points. For test campaigns 2, the product gas measurement was conducted at 8 measurement points and for test campaign 3 at 10 measurement points. Tar was measured for all test campaigns at the lower sample point, but only for test campaign 3 along the height, from measurement point number 6 to 9. Through the measurement program carried out it was possible to get an insight into the effects of the upper gasification reactor regarding the change of product gas components and tar reduction. Based on these results, main influencing parameters like temperature, bed material and height of the column could be figured out.

2. Materials and methods

2.1. Advanced DFB steam gasification reactor system

Due to the initiation to improve the gas-solid contact in the DFB steam gasification pilot plant at TU Wien, an advanced reactor design was developed. Based on continuous ongoing research, a solution was found to increase the contact time between downward flowing hot bed material particles with upwards flowing product gas [11,12]. The advanced design of the 100 kW_{th} DFB steam gasification pilot plant went into operation in 2014 [13]. In the advanced reactor concept (see Fig. 3) the gasification reactor is designed as bubbling bed in the lower part and operates as counter-current column with turbulent fluidized bed zones in the upper part. Therefore, the upper gasification reactor is equipped with constrictions, which allow an increased hold-up of bed material along the height of the reactor. Thus, the residence time for fuel conversion can be increased and the interaction of catalytic active hot bed material particles with the product gas can be enhanced. In addition, the high temperatures in the counter-current column have a positive effect on tar reduction. This was also stated by Pfeifer et al. [14], who recommended high operating temperatures (>900 °C) and increasing gas residence times for sufficient thermal tar cracking. Thus, the conversion efficiency can be increased [10]. Furthermore, the separation system on top of the reactors was improved through the installation of gravity separators prior to cyclones. Due to the fact, that the gas and particle velocities in gravity separators are smaller compared to cyclones, the use of softer bed materials than olivine or quartz like limestone is possible without continuously refilling of fresh bed material [15]. At the prevailing conditions in the gasification reactor system, calcium

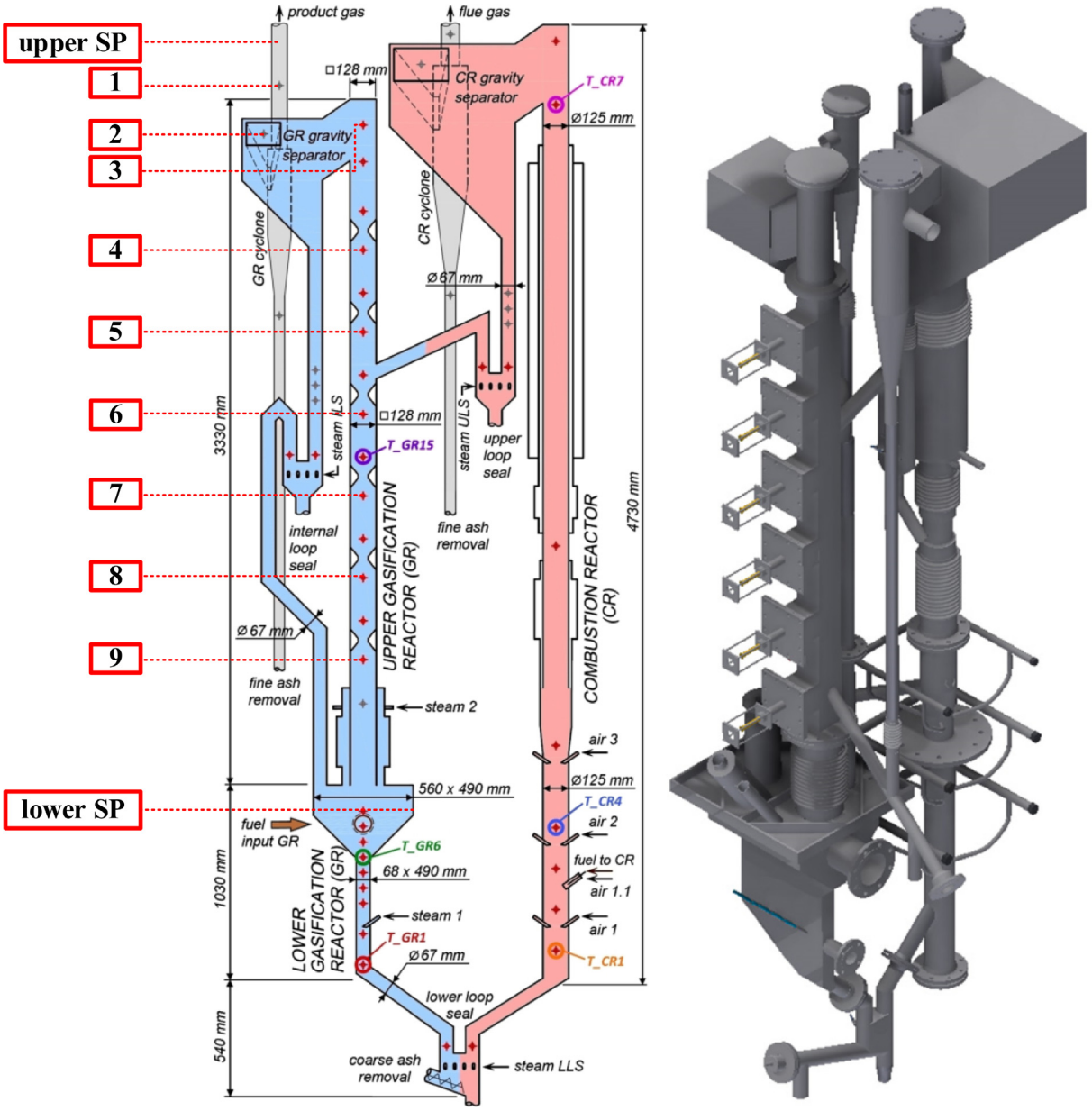

Fig. 3. Sketch indicating dimensions (left) and 3D drawing of the reactor system (right).

carbonate ($CaCO_3$) reacts to calcium oxide (CaO). Due to the fact, that $CaCO_3$ as well as CaO exhibit a very low attrition resistance, a smooth particle separation system is necessary to balance this unfavorable characteristic. Fines smaller than 5–80 μm, which pass the gravity separators are removed via cyclones. Fig. 3 shows the two reactors, which are connected through an upper loop seal (ULS) and a lower loop seal (LLS). In this way, the global solids loop is closed. The solid loop starts in the CR, where solids are entrained, separated from the flue gas and then sent to the GR via the ULS. From the GR, the solids flow back to the CR via the LLS. The internal circulation in the GR is performed via the internal loop seal (ILS). The lower part of the GR (bubbling bed) is constructed like a Y shape. The Y like shape originates from the idea of realizing a bubbling bed regime with a low steam volume flow. The nozzle for the steam input is positioned at the narrow part of the bubbling bed chamber (steam 1). Since the cross section at the narrow part is smaller, the volume flow of steam required to attain a bubbling bed regime is low. The constriction unit (upper GR) with six adjustable constriction modules is positioned above the bubbling bed as explained before. The combustion reactor is designed as fast fluidized bed. The three-staged combustion air feed to the CR allows to increase the amount of combustion air without influencing the bed material circulation rate. Cold flow model investigations showed, that above the secondary combustion air inlet (air 2) the fluidization regime changes from a turbulent regime to a fast bed with an effective pneumatic conveying of particles. By setting the volume flow rates of the primary (air 1) and secondary (air 2) combustion air and the loop seal fluidization, the global bed material circulation rate can be adjusted. The tertiary combustion air volume flow (air 3) can be changed without influencing the bed material circulation since the inlet is situated too high as to have an influence on the bed material level inside the combustion reactor [16].

The advanced 100 kW_{th} DFB steam gasification pilot plant at TU Wien has a height of 4.7 m for the combustion reactor and 4.3 m for the gasification reactor. The combustion reactor is designed as a cylindrical reactor and has an inner diameter of 125 mm. The actual

reactor height of the CR was limited by the given space in the technical laboratory. The lower part of the GR (bubbling bed) has a Y-like shape with a cross sectional area of 68 mm times 490 mm at the narrow part and 560 mm times 490 mm at the extended part. So, the cross section of the bubbling bed changes with the height. The upper gasification reactor is square-shaped and has a cross sectional area of 128 mm times 128 mm. The entire pilot plant has a height of 7 m in total. The whole facility, which includes the fuel supply system, a control room and equipment for gas cooling, cleaning and measurement, covers two floors of around 35 m^2 each.

In Fig. 4 the upper part of the DFB steam gasification pilot plant with the two fuel hoppers is shown and in Fig. 5 the lower part of the pilot plant with the fuel feeding screw and some ash removal containers can be seen. Coarse ash, which accrues during test runs is withdrawn in the lower part of the system. This removal of coarse ash is especially relevant, when ash-rich fuels are used (for more information see Ref. [17]). First results of initial experimental campaigns with the 100 kW_{th} advanced DFB steam gasification pilot plant at TU Wien can be found in Refs. [10,18]. During the last years, various investigations on the advanced 100 kW_{th} pilot plant have been conducted. Fuchs et al. [19] investigated the sorption enhanced reforming process to produce a hydrogen rich gas with

Fig. 4. Upper part of the 100 kW_{th} gasification pilot plant at TU Wien.

Fig. 5. Lower part of the 100 kW_{th} gasification pilot plant at TU Wien.

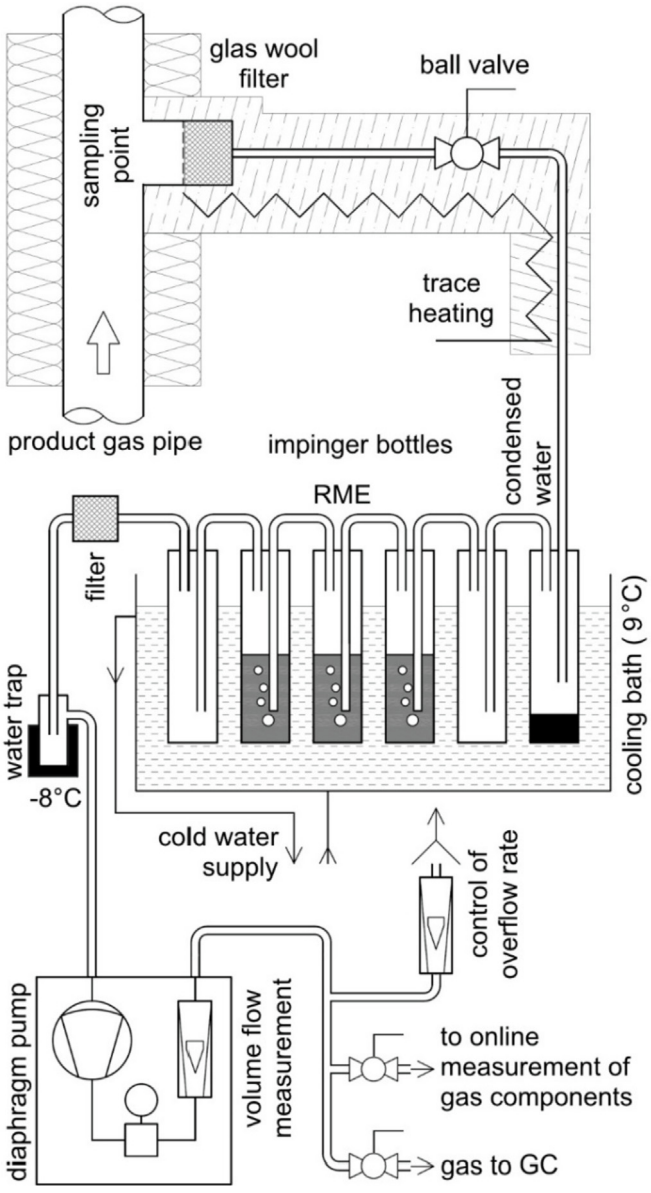

Fig. 6. Gas cleaning line for online measurement of the main product gas components.

the reactor system by inherent CO_2 looping. A variation of bed materials and their influences on product gas quality was investigated by Mauerhofer et al. [15]. And, an extensive fuel variation was presented by Benedikt et al. [20].

2.2. Online measurement equipment

The pilot plant is equipped with a programmable logic controller (PLC). The PLC continuously measured and recorded all relevant flow rates, temperatures, pressures and the main gas components like H_2, CO, CO_2 and CH_4. All process media inputs were measured with variable area flow meters manufactured by the company KROHNE. Temperatures were measured via thermocouples and pressures were quantified by pressure sensors. The volume flow rates of the product gas and flue gas were measured via pressure measuring orifices. The construction type of the pressure measuring orifices was a quarter circle nozzle. The flow rates were calculated based on the guideline VDI/VDE 2041 [21]. The main gas components were analyzed online by a Rosemount NGA2000 measurement device. C_2H_4, ethane (C_2H_6), propane (C_3H_8) and nitrogen (N_2) were analyzed by a gas chromatograph (Perkin Elmer ARNEL – Clarus 500) every 12–15 min. To protect the measurement equipment from contaminants, the product gas had to be cleaned before the measurement. Therefore, it was filtered with a glass wool filter and washed with rapeseed methyl ester (RME) to eliminate condensable components like water and tar (see Fig. 6). RME is used as solvent, because it corresponds to solvents typically used in industrial scrubbing systems [22,23]. Due to that reason, RME was used as solvent for the product gas generated with the pilot plant to simulate industrial conditions. A more detailed description of the measurement devices is given in Refs. [24,25].

2.3. Offline measurement equipment

The offline measurement equipment is based on sampling and determining the contents of dust, char and tar in the product gas afterwards in the laboratory. For the measurement, samples were taken isokinetically with impinger bottles to condense and dissolve hydrocarbons following the suggested procedure of the tar protocol [26] (see Fig. 7). According to the tar protocol, isopropanol should had been used as solvent. However, for the conducted experiments, toluene was used as solvent, because it showed a higher solubility

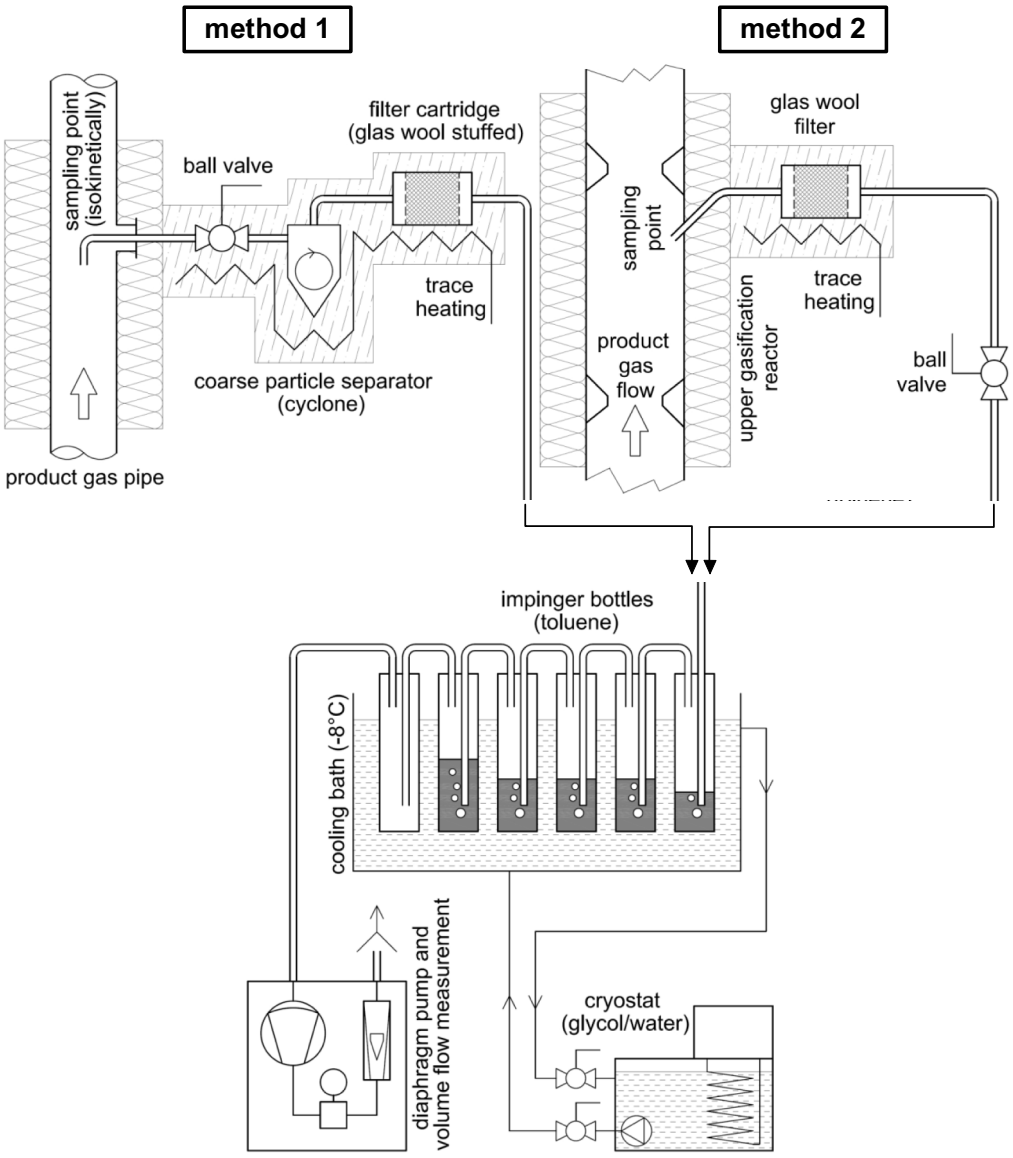

Fig. 7. Offline tar sampling scheme.

than isopropanol. The mass of tar (mostly tar compounds with a high molecular weight) which is left after vacuum evaporation of the solvent is summarized as “gravimetric” tar. Tar compounds with a medium molecular weight like naphthalene are analyzed with a gas chromatograph coupled with mass spectrometry (GC/MS). A more detailed description of the measurement and analysis procedure is given in Refs. [27,28]. The advantage of using toluene as solvent was, that the simultaneous measurement of the water content was possible. However, the use of toluene as solvent excluded its detection and also the measurement of benzene and xylene was difficult within this setup. Due to that, all tar contents are presented without benzene, toluene, ethylbenzene and xylene (BTEX) in this work. The contents of solid particles like char and dust were determined by using a small cyclone with a quartz wool stuffed filter cartridge. It has to be mentioned, that two different measurement methods were used to determine the tar contents at different measurement points along the height. Tar contents at the USP were measured with the method 1 shown in Fig. 7. For “method 1” also tar in the filter was leached out and added to the total content of tar. All other tar contents were determined with the same method, but tar together with particles in the cyclone and filter was not leached out and therefore could not be added to the total tar amount. This method is called “method 2”. In general, the tar measurement along the height was conducted from top to bottom or rather said from low to high tar content.

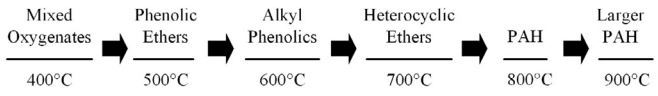

Fig. 8. Tar maturation process scheme proposed by Elliott.

2.4. Classification of tar compounds and definition of the tar dew point

In general, the classification of tar can be conducted according to different systems. Within this paper, the classification systems proposed by Milne et al. [29] and Rabou et al. [30] were used. The two classification systems propose to divide tar compounds into different classes according to different parameters. Milne et al. defined tar regarding their temperature of formation into primary, secondary and tertiary tar compounds. Primary tar products occur between 400 and 700 °C and are characterized by oxygenated compounds. Secondary tar compounds are formed at higher temperatures of around 700–850 °C. They mainly include phenols, which are problematic in the producer gas of biomass gasification and other mono-aromatic hydrocarbons. Tertiary tar forms at temperatures between 850 and 1000 °C and includes predominantly aromatics, which arise out of polyaromatic hydrocarbons (PAH) [31]. In Fig. 8 the transition scheme of tar compounds depending on temperature proposed by Elliott is shown [32].

In contrast to that, Rabou et al. classified tar according to physical properties [30]. In Table 1, the two mentioned classification systems of detected GC/MS tar compounds are displayed. Class I tar compounds are very heavy in molecular weight and cannot be detected by GC. One assumption regarding the classification system of Milne et al. has to be mentioned. Partially, some tar compounds occur in two classes. If that was the case, it was decided to divide the total amount of this tar compound and count halve of it to each of the referring classes. Another noteworthy point is that the tar

Table 1
Detected GC/MS tar compounds according to Rabou and Milne et al. classification [29,30].

GC/MS compounds	Rabou class	Milne class	GC/MS compounds	Rabou class	Milne class
none	Class I (heavy tar)	-			
phenol	Class II (heterocyclic aromatics)	p/s	naphthalene	Class IV (light PAH; 2,3-ring)	s/t
2-methylphenol		p/s	2-methylnaphthalene		s
4-methylphenol		p/s	1-methylnaphthalene		s
2,6-dimethylphenol		p	1-vinylnaphthalene		s
2,5&2,4-dimethylphenol		p	2-vinylnaphthalene		s
3,5-dimethylphenol		p	biphenyl		s
2,3-dimethylphenol		p	acenaphthylene		t
3,4-dimethylphenol		p	acenaphthene		t
2-methoxy-4-methylphenol		p	fluorene		t
benzofuran		s	anthracene		t
2-methylbenzofuran		s	9-methylanthracene		t
dibenzofuran		s	phenanthrene		t
chinoline		s	4,5-methylenphenanthrene		s
isochinoline		s	1H-indene		s/t
indol		-	1-indanone		
carbazol		-	fluoranthene	Class V (heavy PAH; 2,3-ring)	t
1-benzothiophen		-	pyrene		t
dibenzothiophen		-	benzo[a]anthracene		t
2-methylpyiridin		s	chrysene		t
3,4-methylpyiridin		s	benzo[b]fluoranthene		t
eugenol		p	benzo[k]fluoranthene		t
isoeugenol		p	benzo[a]pyrene		t
phenylacetylene	Class III (1-ring aromatic)	t	benzo[e]pyrene		t
styrene		s/t	benzo[g,h,i]perylene		t
mesitylene		t	dibenz[a,h]anthracen		t
			indeno[1,2,3]pyrene		t
			perylene		t
			coronene		t

p…primary; s…secondary; t…tertiary;
PAH…polyaromatic hydrocarbon;

compounds BTEX are not considered in the results presented below. An important value for the impact of tar formation on downstream equipment of long-term operation of biomass gasification is defined by the tar dew point (TDP). The TDP is calculated with the GC/MS tar compounds via a calculation tool from the Energy Research Centre of the Netherlands (ECN) [33].

Fig. 9. Pictures of investigated materials.

2.5. Investigated materials

For comparison of the presented experiments, softwood (SW) pellets with a relatively low ash content of 0.2 wt.-% and a diameter of 6 mm according to the Austrian standard ÖNORM M 7135 were used as fuel. In Table 2 the proximate and ultimate analysis of the softwood pellets are given.

As mentioned before, the fuel SW pellets were used in all experiments. However, the bed material was changed in each test run. Olivine, quartz, feldspar and limestone were used as bed materials, because they are considered to have the greatest potential for industrial plants. The composition of the bed materials is shown in Table 3 and pictures of the bed materials and the fuel SW pellets are shown in Fig. 9. The Sauter mean diameter displayed in Table 3 is defined as the diameter of a sphere, which has the same volume/surface area ratio like the particle of interest (for more information see the literature [34,35]). Olivine is used as state-of-the-art bed material in industrial-sized plants due to its catalytic activity and quite good attrition resistance. However, a disadvantage of olivine is its high price as well as the limited regional availability. Therefore, research is focused on alternative materials, which are cheaper and easier available worldwide such as quartz, feldspar and limestone. Quartz shows a good attrition resistance and has excellent heat transfer properties. Feldspar, which was used, consisted of a high share of potassium with positive effects on gasification. The bed material limestone is primarily composed of calcite and aragonite, which are two crystallization forms of calcium carbonate ($CaCO_3$) and to a very small amount of other minerals. Regarding to the conducted experiments, limestone was filled into the 100 kW_{th} pilot plant as calcium carbonate ($CaCO_3$). This $CaCO_3$ was transformed to the catalytic active form of calcium oxide (CaO) during the test runs due to the high temperatures in the reactor system. This transformation process is explained in detail by Fuchs et al. [19]. On the one hand, CaO was very catalytic active, which was advantageous for the ongoing gasification reaction. However, on the other hand, it exhibits a low attrition resistance, which was not investigated within this work in detail. To overcome the negative effects of one bed material, mixtures of different bed materials were prepared. The mixing of two different bed materials enabled the supplementing of the properties of two different materials and in this way the creation of a suitable bed material for the gasification.

Table 2
Proximate and ultimate analysis of softwood pellets.

parameter	unit	softwood pellets
ash content	wt.-%$_{db}$	0.2
carbon (C)	wt.-%$_{db}$	50.7
hydrogen (H)	wt.-%$_{db}$	5.9
nitrogen (N)	wt.-%$_{db}$	0.2
sulphur (S)	wt.-%$_{db}$	0.005
chloride (Cl)	wt.-%$_{db}$	0.005
oxygen (O)	wt.-%$_{db}$	43.0
volatiles	wt.-%$_{db}$	85.4
fixed C	wt.-%$_{db}$	14.6
water content	wt.-%	7.2
LHV (dry)	MJ/kg$_{db}$	18.9
LHV (moist)	MJ/kg	17.4

2.6. Validation of process data with IPSEpro

The process data, which was recorded during the test campaigns, was used to calculate mass and energy balances with the process simulation software IPSEpro. Due to the validation of measured data with IPSEpro, results can be depicted in a high-valuable and representative way. A detailed model library, which was developed at TU Wien over many years was used for validation of measured process data [36,37]. The IPSEpro model, which was used for the validation of measured data was developed within the research group. For a detailed evaluation of the presented gasification test campaigns, following key figures were selected. In Eq.

Table 3
Physio-chemical properties of bed materials.

parameter	unit	bed material type			
		limestone	quartz	feldspar	olivine
Al_2O_3	wt.-%	-	-	17.5–18.5	-
$CaCO_3$	wt.-%	95–97	-	-	-
Fe_2O_3	wt.-%	-	-	-	8.0–10.5
K_2O	wt.-%	-	-	14.0–15.0	-
$MgCO_3$	wt.-%	1.5–4.0	-	-	-
MgO	wt.-%	-	-	-	48–50
Na_2O	wt.-%	-	-	0.5–1.0	-
SiO_2	wt.-%	0.4–0.6	99–100	65–66	39–42
trace elements (<0.4 per element)	wt.-%	≤3.1	≤1	≤3	≤5
hardness	Mohs	3	7	6	6–7
sauter mean diameter	mm	0.382	0.300	0.287	0.243
particle density	kg/m^3	2650, 1500[a]	2650	2600	2850
minimum fluidization velocity[b]	m/s	0.08–0.18[c]		0.02–0.05[d]	

[a] Particle density after full calcination.
[b] Mean minimum fluidization velocity of natural olivine.
[c] Particle size between 400 and 600 μm.
[d] Particle size between 200 and 300 μm.

(1) the steam to fuel ratio φ_{SF} is expressed as the mass of steam as fluidization medium and the mass of water in the fuel related to the mass of dry and ash-free fuel. Due to the fact, that steam was used as gasification agent to convert carbonic feedstocks and to ensure comparability of biomass gasification investigations in literature, the steam to carbon ratio φ_{SC} was used (see Eq. (2)). Via the steam-related water conversion X_{H2O}, the consumed water for e.g. CO and H_2 production is set into relation to the sum of water, which is introduced into the GR as gasification agent and fuel water (see Eq. (3)). In Eq. (4) the fuel-related water conversion $X_{H2O,fuel}$ is shown, which gives the amount of water consumed per mass unit of converted fuel during gasification. The cold gas efficiency η_{CG} (see Eq. (5)) is the chemical energy content of gaseous components in the tar- and char-free product gas related to the chemical energy in the fuel, which is introduced into the gasification reactor. All values are based on the lower heating value (LHV). The overall cold gas efficiency $\eta_{CG,o}$ describes the amount of chemical energy in the product gas in relation to the fuel introduced into the gasification and combustion reactor minus appearing heat losses (see Eq. (6)). The product gas yield PGY gives information about the ratio between dry product gas to dry and ash-free fuel, which is introduced into the GR (see Eq. (7)). In Eq. (8) the water gas shift reaction (WGS) is displayed, which represents the most essential homogeneous gas-gas reaction during the gasification process. Another relevant reaction is shown in Eq. (9), which describes the steam reforming of hydrocarbons and is important for the discussion of the measurement results. The decision of the selection of these key figures was taken based on the presentation of the same key figures in literature, like in Refs. [15,38].

3. Results and discussion

In Table 4 the main operating parameters for test campaigns 1, 2 and 3 are shown. The total steam input into the GR was between 13 and 16 kg/h for all three test campaigns. The air input into the CR was between 63 and 73 m^3_{stp}/h for test campaigns 1, 2 and 3. These input mass flows were determined based on calculations of the fluid dynamics in the GR and CR. The temperature "T^a_{mean} GR_{lower}", which is the temperature in bubbling bed, "T GR_{upper}", which represents the temperature of hot bed material re-entering the gasification reactor from the upper loop seal as well as the temperature at the outlet of the combustion reactor "T CR_{outlet}" were in the same range for all test campaigns. The steam to carbon ratio φ_{SC} as well as the steam to fuel ratio φ_{SF} were in the same range for test campaigns 1 and 2, but a little bit higher for test campaign 3. The higher values of φ_{SC} and φ_{SF} of test campaign 3 could be justified by the larger diameter of the quartz particles compared to olivine or feldspar. As shown in the study of Koppatz et al. [37], when investigating coarser particles, usually a higher amount of steam is necessary to enable a sufficient fluidization. Thus, a higher φ_{SC} as well as φ_{SF} had to be set for test campaign 3. Fig. 10 shows a comparison of the average temperature profiles along the height of the combustion and the gasification reactor of test campaigns 1, 2 and 3. The temperatures at the top of the combustion reactor were about 950–970 °C. These temperatures are approximately the temperatures of the hot bed material coming from the combustion reactor and entering the upper loop seal. The temperatures in the upper and lower gasification reactor were in a range of 800–970 °C. In the bubbling bed, temperatures of around 750–810 °C prevailed. In the upper part of the gasification reactor quite higher

$$\phi_{SF} = \frac{\dot{m}_{steam} + x_{H2O,fuel}\cdot\dot{m}_{fuel}}{\left(1 - x_{H2O,fuel} - x_{ash,fuel}\right)\cdot\dot{m}_{fuel}} \quad \text{steam to fuel ratio} \tag{1}$$

$$\phi_{SC} = \frac{\dot{m}_{steam} + x_{H2O,fuel}\cdot\dot{m}_{fuel}}{x_{C,fuel}\cdot\dot{m}_{fuel}} \quad \text{steam to carbon ratio} \tag{2}$$

$$X_{H2O} = \frac{\dot{m}_{steam} + x_{H2O,fuel}\cdot\dot{m}_{fuel} - x_{H2O,PG}\cdot\dot{m}_{PG}}{\dot{m}_{steam} + x_{H2O,fuel}\cdot\dot{m}_{fuel}} \quad \text{steam} - \text{related water conversion} \tag{3}$$

$$X_{H2O,fuel} = \frac{\dot{m}_{steam} + x_{H2O,fuel}\cdot\dot{m}_{fuel} - x_{H2O,PG}\cdot\dot{m}_{PG}}{\left(1 - x_{H2O,fuel} - x_{ash,fuel}\right)\cdot\dot{m}_{fuel}} \quad \text{fuel} - \text{related water conversion} \tag{4}$$

$$\eta_{CG} = \frac{\dot{V}_{PG}\cdot LHV_{PG}}{\dot{m}_{fuel}\cdot LHV_{fuel}}\cdot 100 \quad \text{cold gas efficiency} \tag{5}$$

$$\eta_{CG,o} = \frac{\dot{V}_{PG}\cdot LHV_{PG}}{\dot{m}_{GR,fuel}\cdot LHV_{GR,fuel} + \dot{m}_{CR,fuel}\cdot LHV_{CR,fuel} - \dot{Q}_{loss}}\cdot 100 \quad \text{overall cold gas efficiency} \tag{6}$$

$$PGY = \frac{\dot{V}_{PG}}{\dot{m}_{GR,fuel,daf}} \quad \text{product gas yield} \tag{7}$$

$$CO + H_2O \rightleftharpoons CO_2 + H_2 \quad \text{water gas shift reaction} \tag{8}$$

$$C_aH_b + a\,H_2O \rightleftharpoons a\,CO + \left(a + \frac{b}{2}\right)H_2 \quad \text{steam reforming reaction} \tag{9}$$

Table 4
Main operating parameters for test campaigns 1, 2 and 3.

parameter	unit	test campaign		
		1	2	3
fuel type to GR	-	softwood	softwood	softwood
total steam to GR	kg/h	13.4	13.8	15.7
fuel power to GR	kW	102	101	101
total air to CR	m^3_{stp}/h	63.0	72.6	69.0
bed material	wt.-%	mixture of 50/50 (olivine/limestone)	mixture of 50/50 (feldspar/limestone)	100 (quartz)
T_{mean}[a] GR_{lower}	°C	815	797	805
$T\ GR_{upper}$	°C	941	967	944
$T\ CR_{outlet}$	°C	950	977	947
φ_{SF}	kg_{H2O}/kg_{fuel}	0.76	0.78	0.87
φ_{SC}	kg_{H2O}/kg_{C}	1.49	1.53	1.72

[a] Mean temperature in the GR bubbling bed at fuel feeding position.

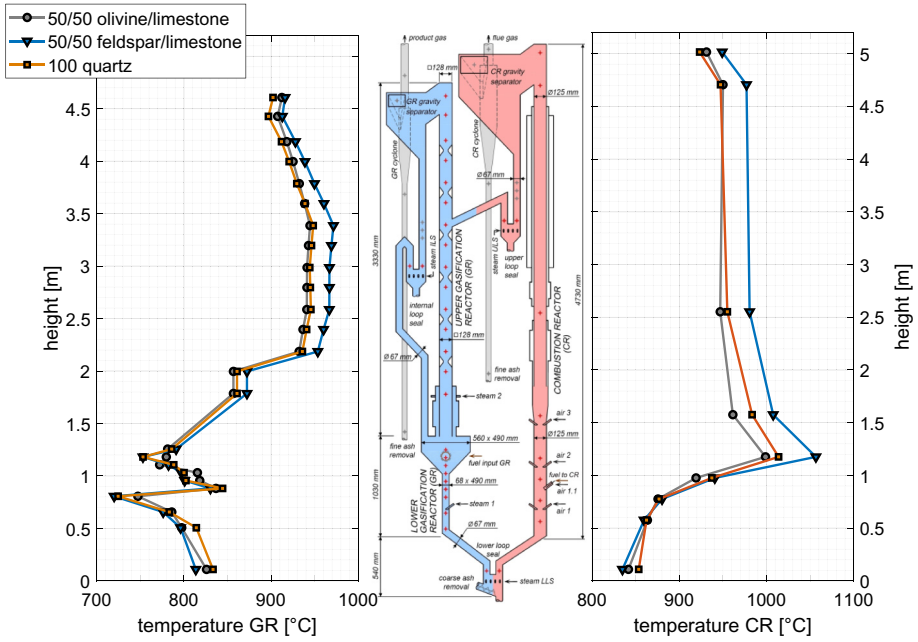

Fig. 10. Overview of the average temperature profiles of test campaigns 1 (grey), 2 (blue) and 3 (orange); left side: gasification reactor, right side: combustion reactor.

temperatures of 900–970 °C were measured. The graphs in Figs. 10–12 were created with the software tool Matlab.

Figs. 11 and 12 display a comparison of the average pressure profiles of the GR and CR of all three test campaigns along the height. It can be seen, that the pressure profiles of all three test campaigns have a similar course along the height.

3.1. Influence of different bed materials on product gas composition along the height

In Figs. 13–15 the results of the product gas composition of test campaigns 1, 2 and 3 are displayed. On the left side, the gasification reactor with the location of the measurement points for the gas composition along the height is shown. In the middle, the formation or reduction of higher hydrocarbons in the product gas, e.g. C_2H_4 and C_2H_6 is shown and on the right side, the main product gas components are displayed. For CO, CO_2 and CH_4 the online data as well as the data of the Perkin Elmer ARNEL – Clarus 500 gas chromatograph are shown. C_3H_8 is not displayed in the graphs, because a value near 0 vol.-% was measured for all three test campaigns. In Fig. 13 test campaign 3, where 100 wt.-% catalytically inactive quartz was used as bed material, is displayed. It is evident, that H_2 showed an increasing trend, whereas CO, C_2H_4 and C_2H_6 were decreasing with increasing height of the gasification reactor. Here, thermal impacts played a much higher role than catalytic impacts, which was the case for test campaigns 1 and 2. Through the increasing temperatures along the height of the GR (see Fig. 10) in combination with the implemented constrictions, the gas-solid

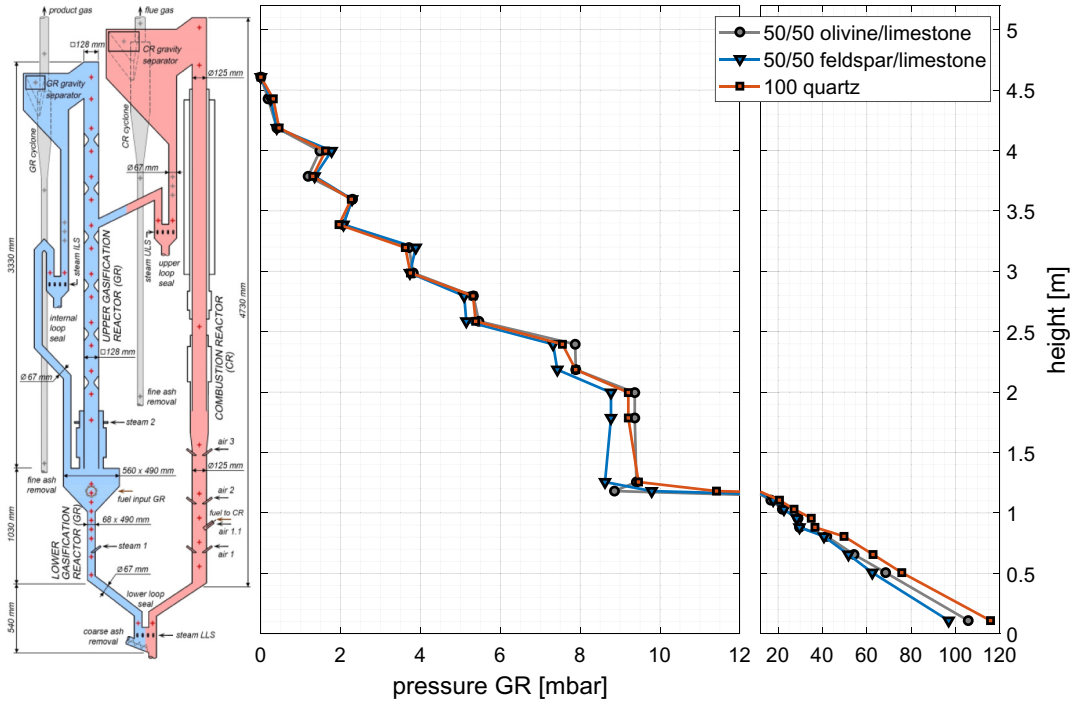

Fig. 11. Overview of the average pressure profiles of the GR of test campaigns 1 (grey), 2 (blue) and 3 (orange).

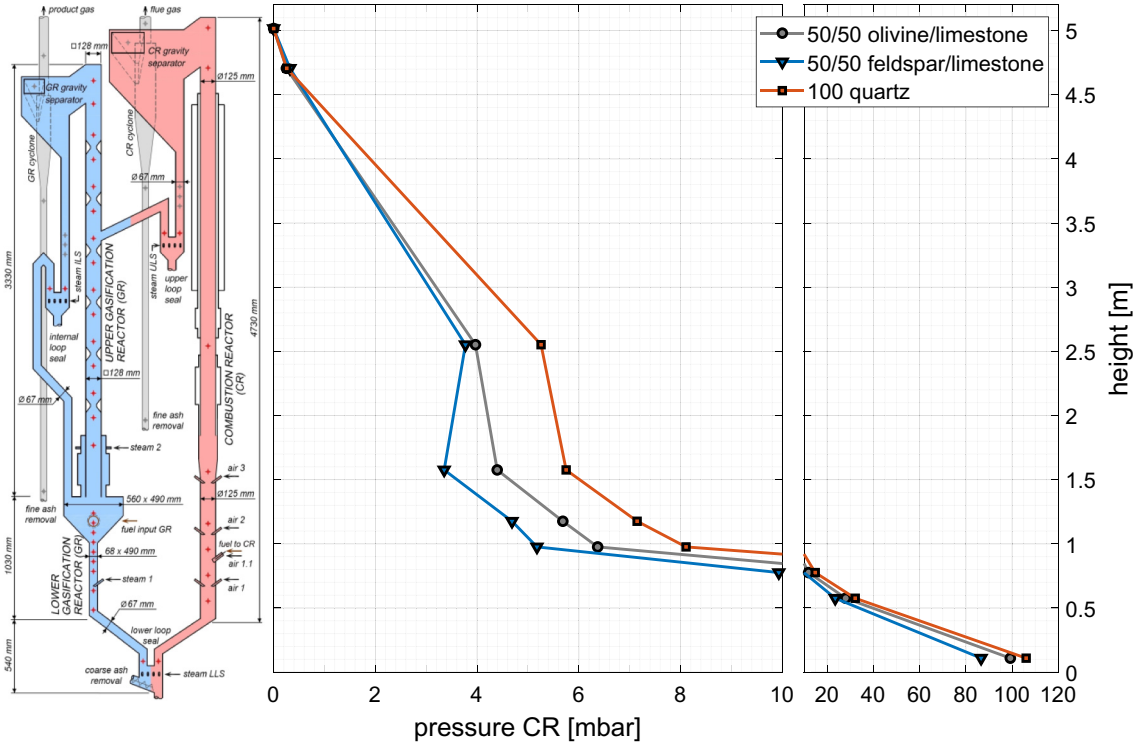

Fig. 12. Overview of the average pressure profiles of the CR of test campaigns 1 (grey), 2 (blue) and 3 (orange).

interaction of hot bed material particles with the product gas was enhanced. Thus, thermal cracking reactions of higher hydrocarbons took place more effectively, which increased the conversion efficiency. Especially, after the entrance of regenerated hot bed material from the combustion reactor, a change in the course of H_2, CO and CO_2 was detected, because from this point the bed material exhibited its highest impact regarding the interaction due to the bed material stream coming from the combustion reactor. CH_4 showed a slight decrease in the lower part of the GR and remained relatively stable afterwards, which could be explained by a dilution of CH_4 due to the increasing content of H_2 along height. In contrast to test campaign 3, test campaigns 1 and 2 (Figs. 14 and 15)

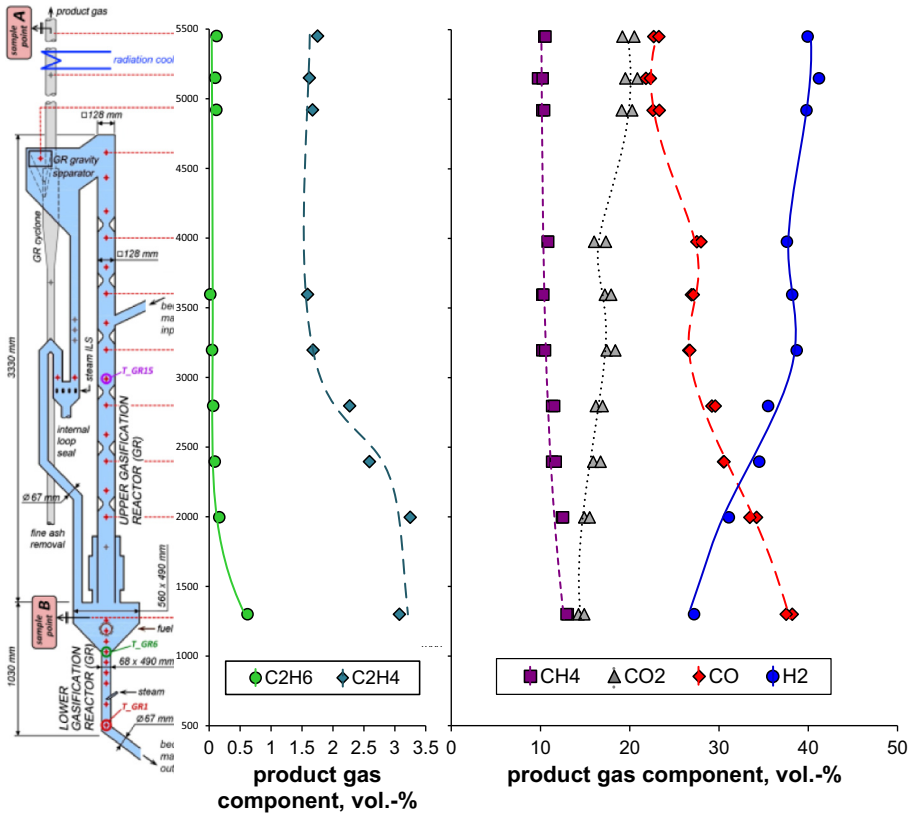

Fig. 13. Product gas composition of gasification of SW with 100 wt.-% quartz as bed material along the height.

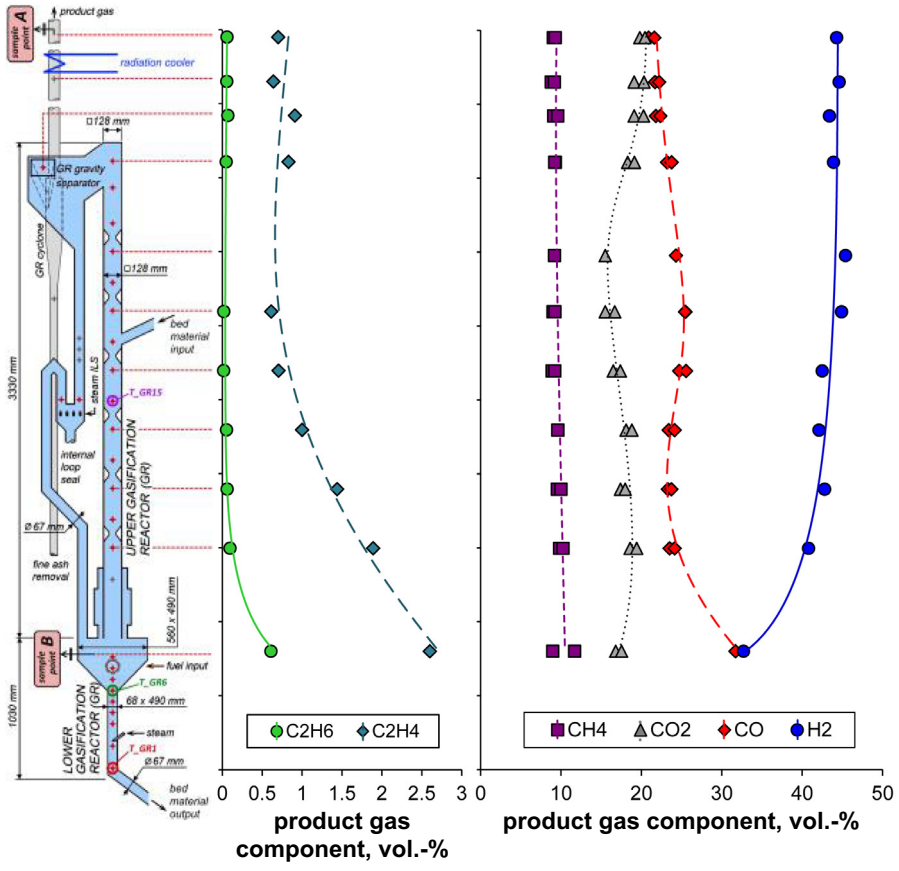

Fig. 14. Product gas composition of gasification of SW with a mixture (50/50 wt.-%) of olivine and limestone as bed material along the height.

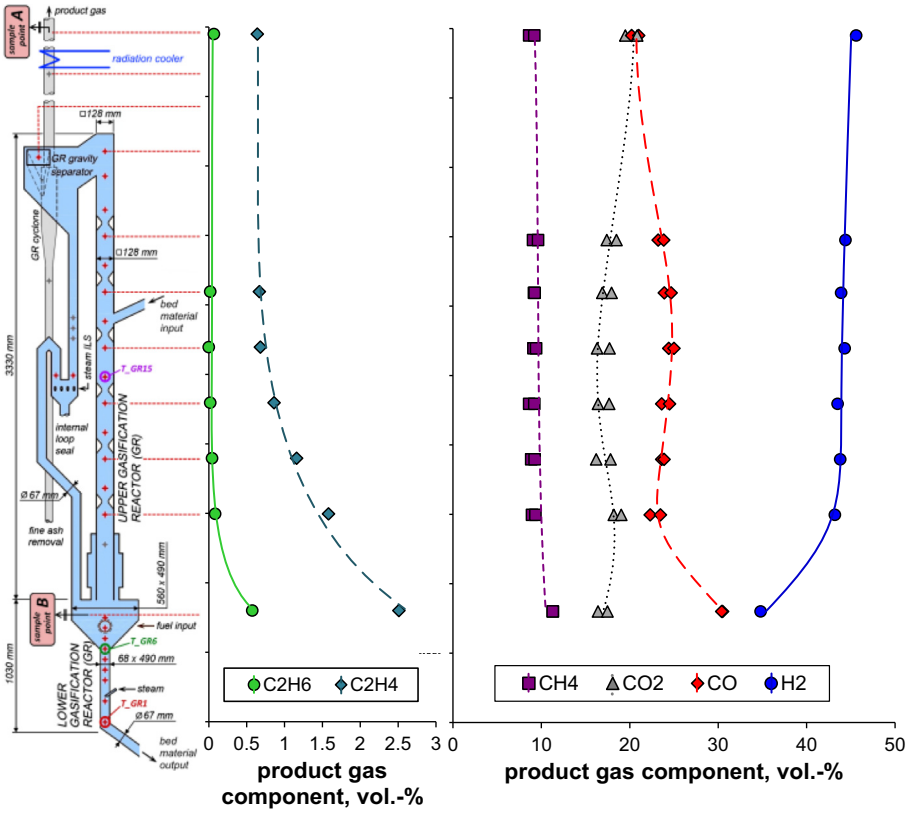

Fig. 15. Product gas composition of gasification of SW with a mixture (50/50 wt.-%) of feldspar and limestone as bed material along the height.

indicated a relatively similar course of product gas components along the height of the gasification reactor. The addition of limestone to olivine and feldspar improved the catalytic activity and thus favoured the ongoing chemical reactions. The decreasing trend of higher hydrocarbons, like C_2H_4 and C_2H_6 along height of the gasification reactor could be explained by the steam reforming reaction (see Eq. (9)), which converted hydrocarbons into CO and H_2. In addition, the water gas shift reaction (see Eq. (8)) was enhanced, which resulted in a rising formation of H_2 and a decrease of CO at the same time. Therefore, higher contents of H_2 and lower contents of higher hydrocarbons like C_2H_4 could be generated.

3.2. Tar evolution along the height of the gasification reactor

In Fig. 16 tar formation and destruction along the height of test campaign 1 with a mixture of olivine and limestone (50/50 wt.-%) as bed material is shown. The figure includes the course of class II, III, IV and V as well the course of gravimetric and GC/MS tar along the height. These tar contents were measured with "method 2" (see Fig. 7). For test campaigns 2 and 3 tar was only measured at the USP with "method 1" (see Fig. 7). These tar values are presented and discussed in Table 5.

As can be seen in Fig. 16, all tar classes show a decreasing trend along the height of the counter-current column. Class IV tar compounds occupied the largest part of GC/MS tar. This was also reported by van der Meijden et al. [39] by investigating gasification of wood with olivine. On the one hand, this could be explained by the stability of naphthalene. On the other hand, the decomposition of higher tar compounds (class V) resulted in the formation of lighter PAHs like naphthalene (class IV). Class III as well as class II tar compounds decreased with increasing height of the counter-current column as well. This could be justified by the enhanced contact of active bed material particles with the product gas, which influenced the conversion efficiency and therefore minimized tar formation. In Fig. 17 it can be seen, that the trend of tar classes proposed by Milne et al. is quite similar to that proposed by Rabou et al. Tertiary tar compounds showed a decreasing trend with increasing reactor height of the gasification reactor. This phenomenon can be seen in Fig. 16 for class V tar compounds as well. Both classes, the tertiary tar class and the class V tar are composed of heavy, high molecular weight compounds. These compounds could be reduced with increasing conversion efficiency as explained before as well as increasing temperatures, which is also shown in the work of Devi et al. [40]. At the same time, secondary tar compounds decreased and primary tar compounds were almost not formed.

In Fig. 18 the main observed GC/MS tar compounds with increasing height of the counter-current column of the gasification reactor are shown. The amount of naphthalene is referred to the upper X-axis, whereas the amount of all other compounds are referred to the lower X-axis, because naphthalene occupies the major amount of the depicted GC/MS tar compounds. The total amount of naphthalene decreased with increasing reactor height. Styrene, acenaphthylene, anthracene and 1H-indene, which are as a whole compound or partially a part of the tertiary tar class showed a declining trend with increasing height of the counter-current column. Phenol, which belongs to the primary as well as the secondary tar class, was extremely low near a value of 0 $g/m^3_{,stp}$. This phenomenon could be again explained by the positive effects of the counter-current column of the gasification reactor of the advanced design. The previous classic design of the gasification reactor was composed of a bubbling bed in the lower part with a freeboard in the

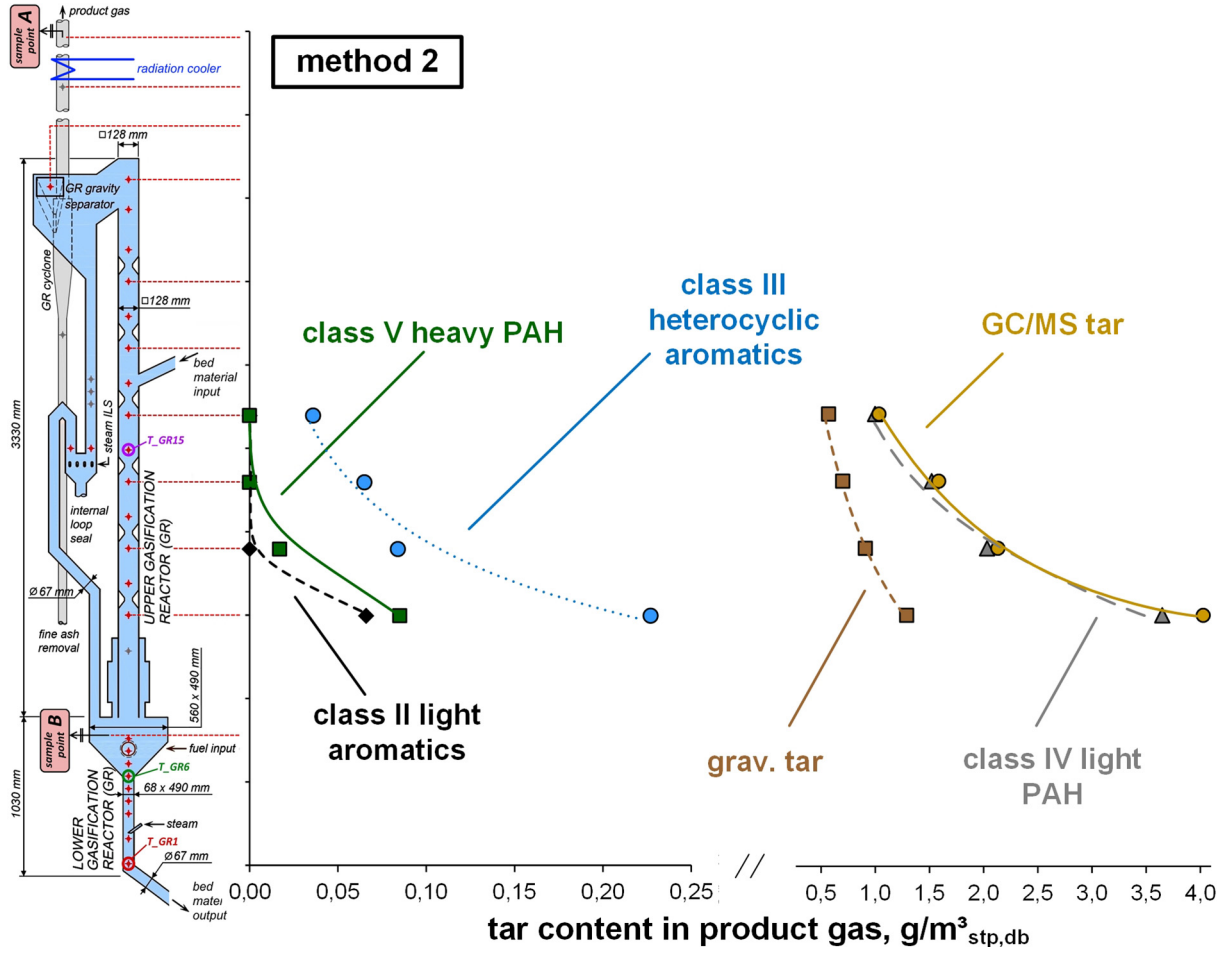

Fig. 16. GC/MS tar classified according to different properties of gasification of SW with a mixture (50/50 wt.-%) of olivine and limestone as bed material along the height.

upper part. Due to that, the contact-time between bed material particles and product gas was much lower, which resulted in a reduced tar conversion compared to the advanced design [41]. This effect could be seen in the work of Koppatz et al., who investigated the gasification of wood with olivine as bed material in the classic design. In this experiments phenol was formed indeed [42].

3.3. Key figures for gasification test campaigns

Table 5 shows a selection of operation parameters and important indicating key figures for the gasification test campaigns 1, 2 and 3. The product gas yield PGY was higher, when limestone was added (test campaigns 1 and 2). This can be explained by longer residence times of char particles in the advanced design of the gasification reactor as well as by the presence of CaO, which supports the gasification reactions. This effect resulted also in a higher steam-related water conversion (X_{H2O}). X_{H2O} might have been positively influenced by longer interaction times between gas and particles as well as by the higher catalytic activity of CaO compared to quartz. The fuel-related water conversions $X_{H2O,fuel}$ of all three test campaigns were in a typical range of 0.22–0.26 kg_{H2O}/kg_{fuel}. Similar values can be found in literature during the gasification of softwood with olivine as bed material [10]. The cold gas efficiencies were approximately in the same range for all three test campaigns (70–74%). Due to the catalytic effect of CaO in terms of steam reforming of hydrocarbons, the gravimetric tar contents were lower in test campaigns 1 and 2. Additionally, the high temperatures in the upper part of the gasification reactor had an advantageous effect on tar reduction and consequently on the conversion efficiency. Compared to investigations with the classic design of the DFB steam gasification pilot plant, where 6 g/m^3_{stp} gravimetric tar with softwood and 100 wt.-% olivine was measured (see Ref. [25]), it was possible to reduce the gravimetric tar contents with the advanced design and mixtures of bed materials to 0.53 g/m^3_{stp} and 0.58 g/m^3_{stp}. 5.21 g/m^3_{stp} gravimetric tar was found in case of quartz as bed material. The same effect can be seen for the GC/MS tar contents, which are lower for test campaigns 1 and 2 compared to test campaign 3, where a GC/MS tar content of 11.89 g/m^3_{stp} was formed during the gasification of softwood with 100 wt.-% quartz. This can be explained by the practically non-catalytic activity of quartz. Consequently, the TDPs are lower for test campaigns 1and 2, where catalytic active bed material limestone was added to olivine and feldspar, compared to test campaign 3. The dust contents of campaigns 1 and 2 were higher than the dust content of campaign 3. This can be explained by the type of bed material. The low abrasion resistance of limestone/CaO resulted in higher dust contents for the bed material mixtures of olivine and feldspar with limestone. Conversely, quartz showed good attrition resistance properties, which resulted in a dust content of almost the half, 4.54 g/m^3_{stp}. The char contents of all three test campaigns were in the same range. Compared to former test campaigns with the classic design, where around 30 g/m^3_{stp} of char by gasifying wood with olivine as bed material was formed, the values of test campaigns 1,2 and 3 are quite low [43]. This can be explained by the advanced design of the

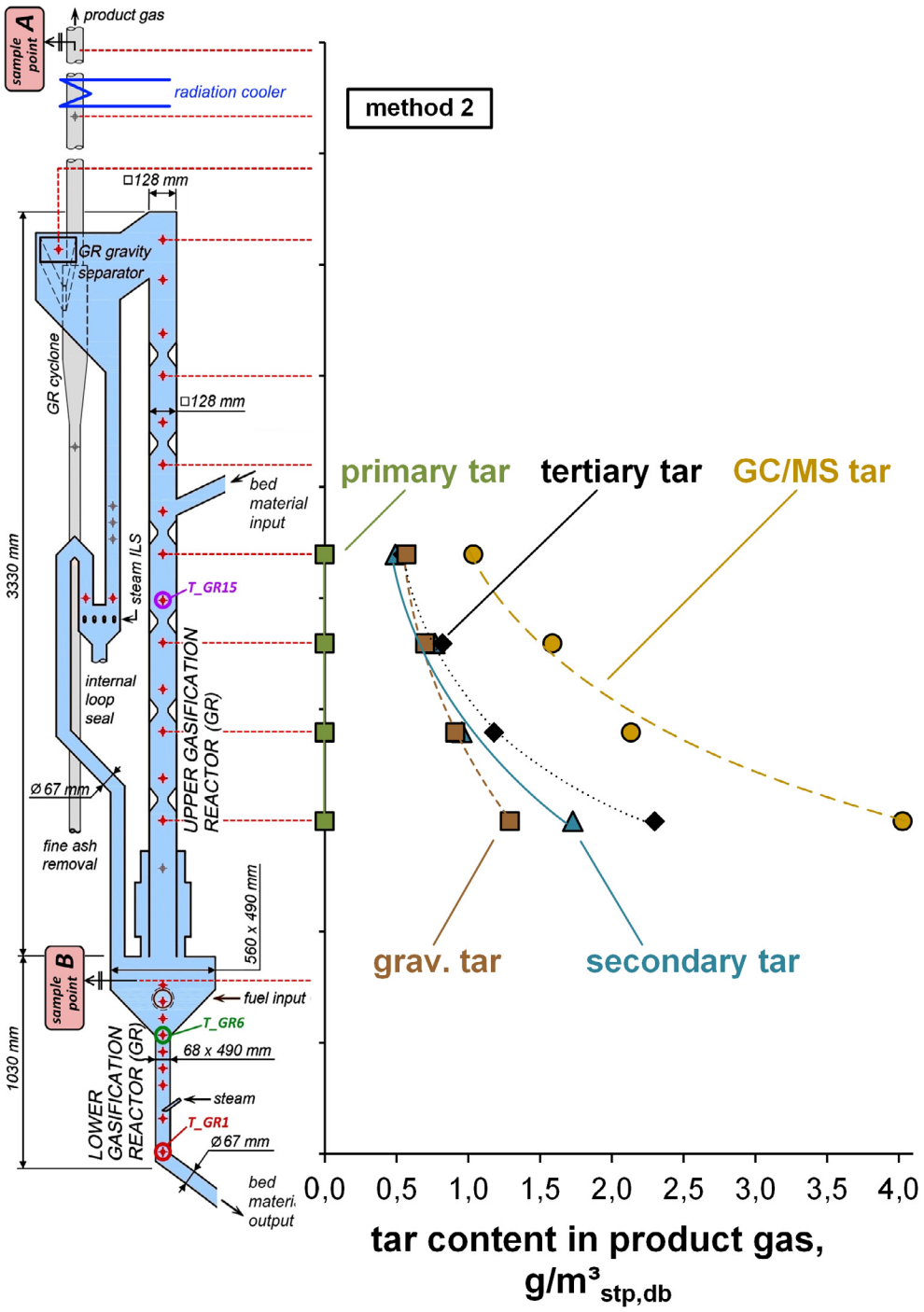

Fig. 17. GC/MS tar classified according to temperature of formation of gasification of SW with a mixture (50/50 wt.-%) of olivine and limestone as bed material along the height.

pilot plant. Firstly, the improved separation system and secondly the design of the gasification reactor influenced the char contents. Due to the counter-current column of the gasification reactor the interaction of gas and particles was enhanced, which resulted in longer residence times. Thus, the conversion efficiency was increased and therefore the char contents were lower.

4. Conclusions and outlook

Within this work, three gasification test campaigns of softwood as fuel with different bed materials were carried out in the advanced 100 kW_{th} DFB steam gasification pilot plant at TU Wien. The focus of the investigations laid on the measurement of the product gas and tar contents along the height of the counter-current column of the gasification reactor. Based on these extensive measurements, it could be found, that the counter-current column has indeed a positive effect on the increase of the gas-solid contact as well as an increase of the conversion efficiencies. The H_2 contents increased with increasing height of the counter-current column, whereas the CO, C_2H_4 and C_2H_6 contents decreased. CH_4 remained relatively stable along the height of the column. The CO_2 content increased due to the increase of the H_2,

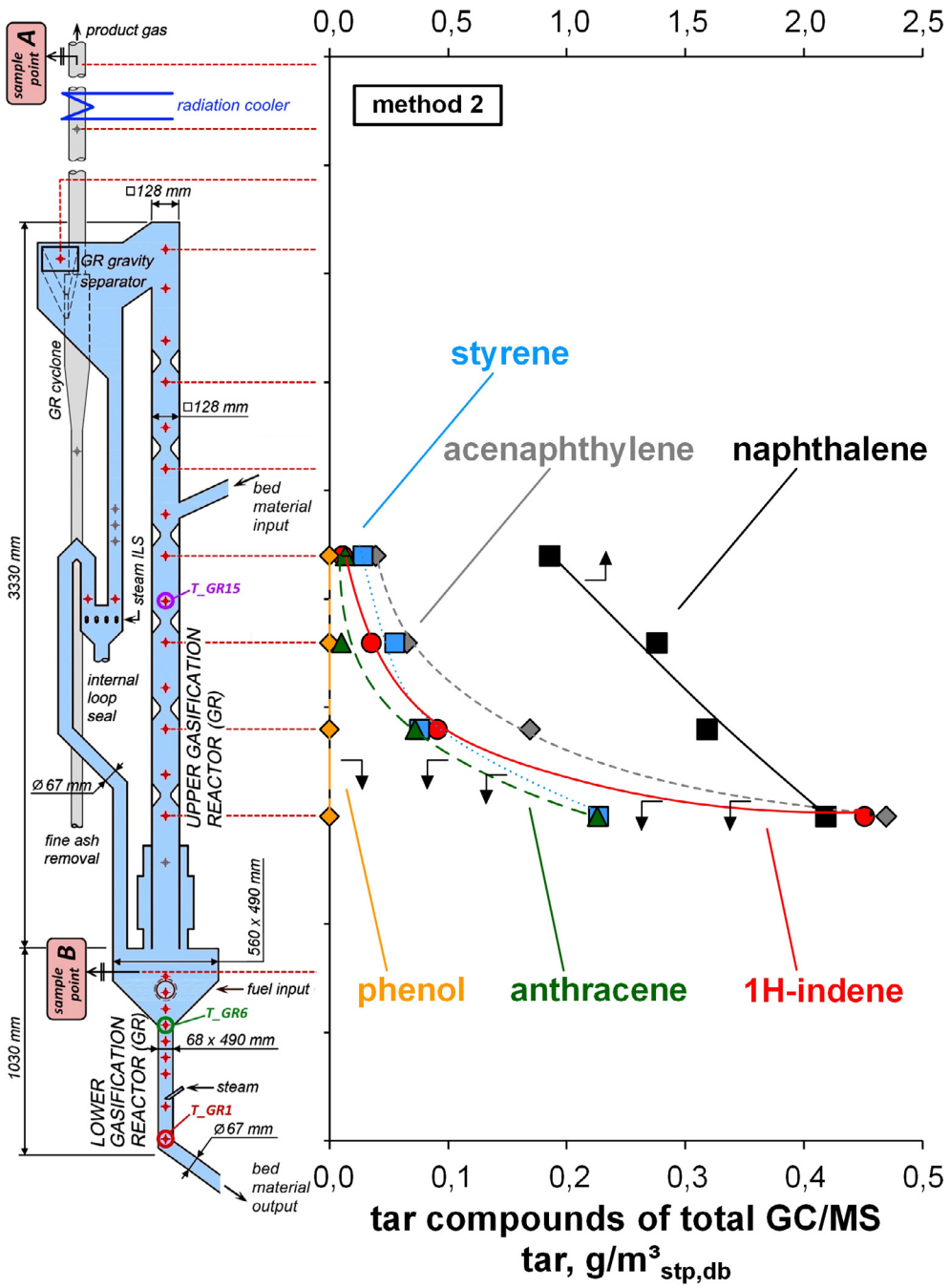

Fig. 18. Tar compounds of total GC/MS tar of gasification of SW with a mixture (50/50 wt.-%) of olivine and limestone as bed material along the height.

Table 5
Operation parameters and key figures of gasification test campaigns 1 to 3.

	test run	1	2	3
bed material mixture		olivine/limestone	feldspar/limestone	quartz
X_{H2O}	kg_{H2O}/kg_{steam}	0.32	0.33	0.25
$X_{H2O,fuel}$	$kg_{H2O}/kg_{fuel,daf}$	0.24	0.26	0.22
η_{CG}	%	87	89	88
$\eta_{CG,o}$	%	74	71	70
PGY	$m^3_{stp,db}/kg_{fuel,daf}$	1.42	1.44	1.34
grav. tar	g/m^3_{stp}	0.53[a]	0.58[a]	5.21[a]
GC/MS tar	g/m^3_{stp}	3.07[a]	2.35[a]	11.89[a]
TDP	°C	123[a]	115[a]	211[a]
dust	g/m^3_{stp}	8.03	7.96	4.54
char	g/m^3_{stp}	4.56	5.76	6.10

[a] Measured at upper sample point via method 1.

which resulted from the WGS reaction. The GC/MS as well as gravimetric tar contents were significantly lower for the bed material mixtures with limestone (test campaigns 1 and 2) compared to test campaign 3, where 100 wt.-% quartz was used. The dust contents of test campaigns 1 and 2 were nearly doubled, when 50 wt.-% limestone was added to the bed material mixture compared to test campaign 3. The use of the advanced design of the 100 kW_{th} pilot plant at TU Wien for the presented test campaigns enabled to generate quite low char contents. The comprehensive measurement of tar at different points along the height of the counter-current column and subsequent classification of GC/MS tar contents was conducted for test campaign 1. A correlation between tar formation and the height of the counter-current column could be observed. The higher the measurement point of the counter-current column and consequent prevailing higher temperatures, the more heavy tar compounds could be reduced. Additionally, the catalytic activity of CaO contributed to the reduction of tar, which is also shown in literature [15].

To sum up, quite high thermal and catalytic forces for reforming and cracking reactions as well as the WGS reaction influenced the change of the gas composition and tar contents along the height of the upper GR. This effect can especially be seen for higher hydrocarbons. Through the proof, that the design of the counter-current column has indeed a great impact on the gas-solid interaction as well as the conversion efficiency, another important effect was figured out during the investigations: the height of the column. As can be seen in Figs. 14 and 15 the significant change of the product gas occurred already in the lower part of the column and then remained relatively constant afterwards. However, the contrast is shown in Fig. 13, where the product gas changed along the whole height of the column. The reason lies in the catalytic activity of the bed material. That means, that for the use of catalytic active bed materials the column could be reduced in length, whereas for the use of non-catalytic active bed materials like quartz the height of the column is of huge relevance. Further investigations could be carried out in a DFB gasification system with reduced height of the upper GR. Additionally, detailed tar measurement of catalytic non-active bed materials like quartz could be carried out along the height of the GR.

Acknowledgement

This work was supported by the European Union's Horizon 2020 research and innovation programme under grant agreement number 764675.

List of abbreviations

CR	combustion reactor
DFB	dual fluidized bed
ECN	Energy Research Centre of the Netherlands
GC/MS	gas chromatography coupled with mass spectrometry
GR	gasification reactor
grav. tar	gravimetric tar
LHV	lower heating value
PAH	polyaromatic hydrocarbons
PGY	product gas yield
SW	softwood
TDP	tar dew point
vol.-%	volumetric percent
WGS	water gas shift
wt.-%	weight percent

List of subscripts

ash	ash carbon
CR	combustion reactor
daf	dry and ash-free
db	dry basis
fuel	fuel to gasification reactor
GR	gasification reactor
H_2O	water
PG	product gas
steam	steam introduced into the gasification reactor
stp	standard temperature and pressure
th	thermal

List of symbols

a,b	stoichiometric factors (−)
$\dot{m}$	mass flow (kg/s)
x	mass fraction
V_{PG}	dry volumetric product gas flow (m^3/s)
X_{H2O}	steam-related water conversion (kg_{H2O}/kg_{H2O})
$X_{H2O,fuel}$	fuel-related water conversion ($kg_{H2O}/kg_{fuel,daf}$)
φ_{SC}	steam to carbon ratio (kg_{H2O}/kg_C)
φ_{SF}	steam to fuel ratio ($kg_{H2O}/kg_{fuel,daf}$)
η_{CG}	cold gas efficiency (%)
$\eta_{CG,o}$	overall cold gas efficiency (%)
Q_{loss}	heat loss (kW)
LHV	lower heating value ($MJ/m^3_{stp,db}$)
PGY	product gas yield ($m^3_{stp,db}/kg_{fuel,daf}$)

References

[1] Codina Gironès V, Moret S, Peduzzi E, Nasato M, Maréchal F. Optimal use of biomass in large-scale energy systems: insights for energy policy. Energy 2017;137:789–97. https://doi.org/10.1016/j.energy.2017.05.027.
[2] Danish energy agency. Energy statistics 2017:vol. 58.
[3] Müller S, Groß P, Rauch R, Zweiler R, Aichernig C, Fuchs M. Production of diesel from biomass and wind power – energy storage by the use of the Fischer-Tropsch process. 2017. https://doi.org/10.1007/s13399-017-0287-1.
[4] Weber G, Rauch R, Hofbauer H. Production of mixed alcohols from biomass-derived synthesis gas using a sulfidized molybdenum catalyst. In: Proc Int Conf Polygeneration Strateg (ICPS13), Vienna, ISBN 978-3-9502754-8-3.
[5] Hofbauer H. Gasification of organic material in a novel fluidization bed system. Proc. of the 1st SCEJ Symposium on Fluidization. 1995. Tokyo.
[6] Hofbauer H, Rauch R, Bosch K, Koch R, Aichernig C. Biomass CHP plant güssing - a success story. Expert meet pyrolysis gasif biomass waste. 2002.
[7] Wilk V, Hofbauer H. Analysis of optimization potential in commercial biomass gasification plants using process simulation. Fuel Process Technol 2016;141:138–47. https://doi.org/10.1016/j.fuproc.2015.07.035.
[8] Gunnarsson I. The GoBiGas project - efficient transfer of biomass to biofuels. In: Proceedings of the international seminar on gasification; 2010. Gothenburg, Sweden.
[9] Schmid JC, Pröll T, Pfeifer C, Hofbauer H. Improvement of gas – solid interaction in dual circulating fluidized bed systems. Proc 9th Eur Conf Ind Furn Boil (INFUB), Estoril, Port 2011:1–13. 2011.
[10] Kolbitsch M. First fuel tests at a novel 100 kWth dual fliuidized bed steam gasification pilot plant. Doctoral thesis. TU Wien; 2016.
[11] Pfeifer C, Schmid JC, Pröll T, Hofbauer H. Next generation biomass gasifier. In: Berlin G, editor. Proc. 19th eur. Biomass conf. Exhib.; 2011.
[12] Schmid JC, Pröll T, Pfeifer C, Rauch R, Hofbauer H. Cold flow model investigation on a modified riser with enhanced gas-solid contact – locating the regions of operation in a fluidization regime map. Proc. 21st Int. Conf. Fluid. Bed Combust., Naples, Italy 2012. 88–87.
[13] Schmid JC. Development of a novel dual fluidized bed gasification system for increased fuel flexibility. Doctoral thesis. TU Wien; 2014.
[14] Pfeifer C. Catalytic decomposition of tar from product gas of a dual fluidised bed biomass steam gasification process. TU Wien, Doctoral thesis; 2005.
[15] Mauerhofer AM, Benedikt F, Schmid JC, Fuchs J, Müller S, Hofbauer H. Influence of different bed material mixtures on dual fluidized bed steam gasification. Energy 2018;157:957–68. https://doi.org/10.1016/j.energy.2018.05.158.
[16] Diem R. Design , construction and startup of an advanced 100 kW dual fluidized bed system for thermal gasification. 2015.
[17] Fuchs J, Müller S, Hofbauer H. Ash related limitations of dual fluidized bed steam gasification. 13 Minisymp Für Verfahrenstechnik 2017:4–7.
[18] Schmid JC, Müller S, Hofbauer H. First scientific results with the novel dual fluidized bed gasification test facility at TU wien. 24th Eur Biomass Conf Exhib 2016;2–6.
[19] Fuchs J, Schmid JC, Benedikt F, Müller S, Hofbauer H, Stocker H, et al. The impact of bed material cycle rate on in-situ CO2 removal for sorption

enhanced reforming of different fuel types. Energy 2018;162:35–44. https://doi.org/10.1016/j.energy.2018.07.199.
[20] Benedikt F, Schmid JC, Fuchs J, Mauerhofer AM, Müller S, Hofbauer H. Fuel flexible gasification with an advanced 100 kW dual fluidized bed steam gasification pilot plant. Energy 2018;164:329–43. https://doi.org/10.1016/j.energy.2018.08.146.
[21] Schmalzl M. Implementierung der MSR- Technik einer 100 kW DUAL FLUID Versuchsanlage zur Vergasung von Festbrennstoffen. n.d.
[22] Hofbauer H, Rauch R, Löffler G, Kaiser S, Fercher E, H. T. Six years experience with the FICFB-gasification process. 12th eur. Biomass conf. ETA florence. 2002. p. 982–5. Italy, Amsterdam.
[23] Kirnbauer F, Wilk V, Hofbauer H. Performance improvement of dual fluidized bed gasifiers by temperature reduction: the behavior of tar species in the product gas. Fuel 2013;108:534–42. https://doi.org/10.1016/j.fuel.2012.11.065.
[24] Kolbitsch M, Schmid JC, Diem R, Müller S, Hofbauer H. Influence of fuel feeding position on sorption enhanced reforming in a dual fluid gasifier, vols. 1–6; 2014.
[25] Schmid JC, Wolfesberger U, Koppatz S, Pfeifer C, Hofbauer H. Variation of feedstock in a dual fluidized bed steam gasifier - influence on product gas, tar content, and composition. Environ Prog Sustain Energy 2012;31:205–15. https://doi.org/10.1002/ep.11607.
[26] Tar Guideline, DIN CEN/TS 15439 2006.
[27] Wolfesberger U, Aigner I, Hofbauer H. Tar content and composition in producer gas of fluidized bed gasification of wood — influence of temperature and. Pressure 2009;28. https://doi.org/10.1002/ep.
[28] van Paasen SVB, Kiel JHA, Neeft JPA, Knoef HAM, Buffinga GJ, Zielke U, et al. Guideline for sampling and analysis of tar and particles in biomass producer gases. 2002.
[29] Milne TA, Evans RJ. Biomass gasifier " tars ": their nature , formation , and conversion. 1998. https://doi.org/10.2172/3726.
[30] Rabou LPLM, Zwart RWR, Vreugdenhil BJ, Bos L. Tar in biomass producer gas, the energy research Centre of The Netherlands (ECN) experience: an enduring challenge. Energy Fuels 2009;23:6189–98. https://doi.org/10.1021/ef9007032.
[31] Morf P, Hasler P, Nussbaumer T. Mechanisms and kinetics of homogeneous secondary reactions of tar from continuous pyrolysis of wood chips. Fuel 2002;81.
[32] Elliott D. Relation of reaction time and temperature to chemical composition of pyrolysis oils. ACS Publ; 1988.
[33] Energy research center of The Netherlands (ECN). 2017. http://www.thersites.nl/completemodel.aspx. [Accessed 12 February 2017].
[34] Pacek AW, Man CC, Nienow AW. On the sauter mean diameter and size distributions in turbulent. Pdf. Chem Eng Sci 2011;53:2005–11.
[35] Filippa L, Trento A, Álvarez AM. Sauter mean diameter determination for the fine fraction of suspended sediments using a LISST-25X diffractometer. Meas J Int Meas Confed 2012;45:364–8. https://doi.org/10.1016/j.measurement.2011.11.009.
[36] Pröll T, Hofbauer H. Development and application of a simulation tool for biomass gasification based processes. Int J Chem React Eng 2008;6. https://doi.org/10.2202/1542-6580.1769. Article A89.
[37] Müller S, Fuchs J, Schmid JC, Benedikt F, Hofbauer H. Experimental development of sorption enhanced reforming by the use of an advanced gasification test plant. Int J Hydrog Energy 2017;42:29697–707. https://doi.org/10.1016/j.ijhydene.2017.10.119.
[38] Benedikt F, Fuchs J, Schmid JC, Müller S, Hofbauer H. Advanced dual fluidized bed steam gasification of wood and lignite with calcite as bed material. Kor J Chem Eng 2017;34:2548–58. https://doi.org/10.1007/s11814-017-0141-y.
[39] Meijden CM Van Der, Veringa HJ, Drift A Van Der, Vreugdenhil BJ. The 800 kWth allothermal biomass gasifier MILENA. 16th Eur Biomass Conf. 2008. p. 2–6.
[40] Devi L, Ptasinski KJ, Janssen FJJG, Van Paasen SVB, Bergman PCA, Kiel JHA. Catalytic decomposition of biomass tars: use of dolomite and untreated olivine. Renew Energy 2005;30:565–87. https://doi.org/10.1016/j.renene.2004.07.014.
[41] Schmid JC, Pfeifer C, Kitzler H, Pröll T, Hofbauer H. A new dual fluidized bed gasifier design for improved in situ conversion of hydrocarbons. Proc Int Conf Polygeneration Strateg 2011:1–10.
[42] Koppatz S, Pfeifer C, Hofbauer H. Comparison of the performance behaviour of silica sand and olivine in a dual fluidised bed reactor system for steam gasification of biomass at pilot plant scale. Chem Eng J 2011;175:468–83. https://doi.org/10.1016/j.cej.2011.09.071.
[43] Wilk V, Aichernig C, Hofbauer H. Waste wood gasification: distribution of nitrogen, sulphur and chlorine in a dual fluidised bed steam gasifier. Int Conf Circ Fluid Bed Technol CFB 2011;10:1–8.